Gold nanoparticle-modulated conductivity in gold peapodded silica nanowires

ARTICLE *in* NANOSCALE · MAY 2012

Impact Factor: 7.39 · DOI: 10.1039/c2nr30549f · Source: PubMed

Nanoscale

Cite this: *Nanoscale*, 2012, **4**, 3660

www.rsc.org/nanoscale

COMMUNICATION

Gold nanoparticle-modulated conductivity in gold peapodded silica nanowires†

Sheng-Bo Wang,[a] Ming-Shien Hu,[b] Shoou Jinn Chang,[a] Cheong-Wei Chong,[cd] Hsieh-Cheng Han,[e] Bohr-Ran Huang,[f] Li-Chyong Chen[e] and Kuei-Hsien Chen*[be]

Received 7th March 2012, Accepted 10th April 2012
DOI: 10.1039/c2nr30549f

We report the enhanced electrical conductivity properties of single gold-peapodded amorphous silica nanowires synthesized using microwave plasma enhanced chemical vapor deposition. Dark conductivity of the gold-peapodded silica nanowires can be adjusted by controlling the number of incorporated metal nanoparticles. The temperature-dependent conductivity measurement reveals that the band tail hopping mechanism dominates the electron transport in the gold-peapodded silica nanowires. The high conductivity in the nano-peapodded nanowires with more embedded gold-nanoparticles can be explained by the higher density of hopping states and shorter hopping distance. These Au-embedded amorphous silica nanowires have provided a new approach to enhance not only the electron conduction, but also the chemical-sensor response/sensitivity.

Introduction

Electron transport in composites of metal nanoparticles embedded in dielectric materials has attracted substantial interest in both fundamental and applied research.[1–7] It has been recognized that the electronic, optical and magnetic properties of metal nanoparticles (NPs) embedded in a dielectric matrix depend mainly on the size and shape of the nanoparticles, the interparticle distance, and the dielectric constant of the surrounding medium.[8] The electronic transport mechanism of metal–dielectric composite films, such as two-dimensional (2D) and three-dimensional (3D) systems, has been studied, in which the conduction mechanism was attributed to electron tunnelling.[9,10]

The transport mechanism of one-dimensional (1D) metal NPs in a dielectric matrix, however, is less studied. Hu *et al.* reported Au nanoparticle-embedded silica nanowire devices with wavelength-dependent and reversible photoresponsive behavior associated with the surface plasmon resonance (SPR) effect.[11] They have potential applications as wavelength selective nanoswitches.[11] Chou *et al.* reported that the electron conduction in single gold-in-Ga_2O_3 peapodded nanowires could be explained by the SPR effect.[12,13] However, despite the reports detailing synthesis and properties, the origins of electron transport behavior in Au-peapodded silica nanowires are still unresolved.[14] Furthermore, the effect of Au nanoparticles on the electronic properties of the nanowires and their accompanying transport mechanism has still not been investigated. In this work, we report that the conductivity of Au-NP peopodded silica nanowires can be modulated by the number of embedded NPs. Moreover, a carrier conduction mechanism of the Au-NP peapodded silica nanowires is proposed, based on a temperature-dependent dark conductivity study. The capability of using this nanowire for oxygen sensing is also demonstrated, and has provided a new approach for future applications in chemical/bio sensors, optoelectronic devices and semiconductor circuits.

Experimental

The Au-peapodded silica nanowires were synthesized by microwave plasma enhanced chemical vapor deposition (MWPECVD) using a microreactor.[11] The single nanowire device was fabricated by focused ion beam (FIB) nanolithography using a methyl cyclopentadienyl trimethyl platinum ($(CH_3)_3Pt(CpCH_3)$) injector to deposit platinum contacts on the SiN_x (200 nm)/Si substrate. The morphology of the Au-peapodded silica nanowires was characterized by field-emission scanning electron microscopy (JEOL 6700). The electrical characteristic of single nanowire devices were carried out using a two-terminal ultralow current leakage probe station at room temperature. A semiconductor characterization system (Keithley model 4200-SCS) was used for the electrical measurements.

Results and discussion

Fig. 1 depicts the FESEM image of an ensemble of Au-peapodded silica nanowires on the SiN_x/Si substrate. To obtain the resistivity of the nanowires and the associated contact resistance of the nanowires

[a]*Institute of Microelectronics & Department of Electrical Engineering, Center for Micro/Nano Science and Technology, Advanced Optoelectronic Technology Center, National Cheng Kung University, Tainan, Taiwan*
[b]*Institute of Atomic and Molecular Sciences, Academia Sinica, Taipei, Taiwan. E-mail: chenkh@pub.iams.sinica.edu.tw*
[c]*Department of Physics, National Taiwan University, Taipei, Taiwan*
[d]*Nano Science and Technology Program, Taiwan International Graduate Program, Academia Sinica, Taipei, Taiwan*
[e]*Center for Condensed Matter Sciences, National Taiwan University, Taipei, Taiwan*
[f]*Institute of Electro-Optical Engineering Department of Electronic Engineering, National Taiwan University of Science and Technology, Taipei, Taiwan*

† Electronic supplementary information (ESI) available. See DOI: 10.1039/c2nr30549f

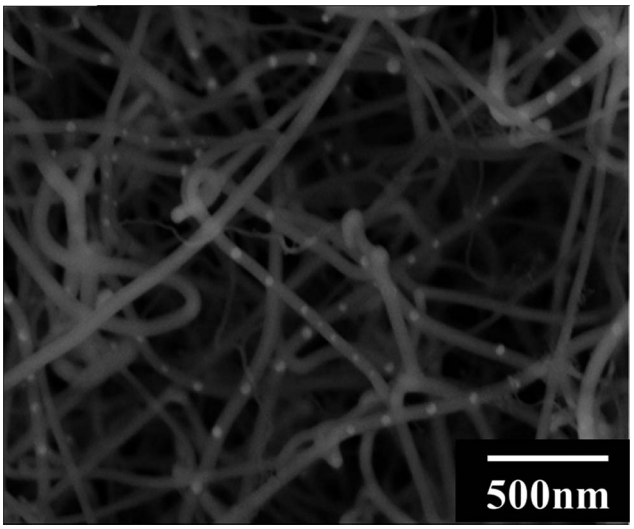

Fig. 1 SEM image of gold peapodded silica nanowires synthesized by MWPECVD.

and Pt electrode, we applied the transmission line method (TLM) and measured the total resistance as a function of the length-to-area ratio. The measured total resistance (R_T) can be described by the relation

$$R_T = 2R_c + \left(\frac{\rho_{NW}}{\pi}\right)\left(\frac{L}{r^2}\right), \quad (1)$$

where R_c is the contact resistance, ρ_{NW} is the sheet resistivity of the plain silica nanowire, L is the length of nanowire between two electrodes, and r is its radius. The R_c and the ρ_{NW} of the plain silica nanowires can be extracted from the intercept and slope of the linear fit, respectively as shown Fig. 2. The contact resistivity (ρ_c) is defined as $\rho_c = R_c A$, where A is the contact area. For individual plain silica nanowires, the contact resistivity (ρ_c) and silica nanowire resistivity were determined to be 1.3×10^{-3} Ω cm^2 and 190 Ω cm by the TLM measurement, respectively. Therefore the resistivity, ρ_{NW} of the single nanowire was calculated by

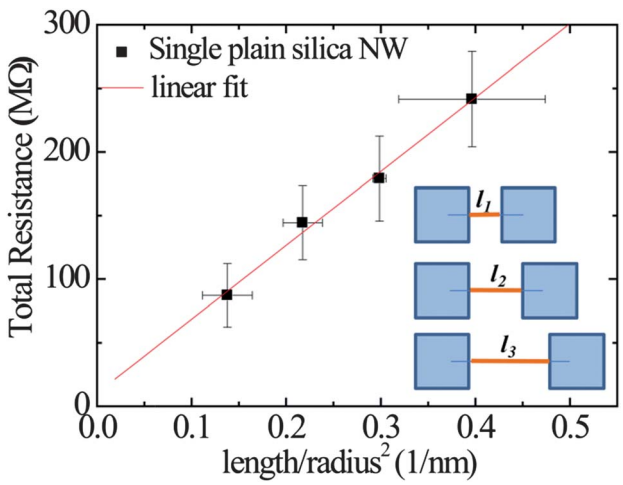

Fig. 2 The total resistance as a function of the length/radius square of single silica nanowire. The inset figure is multi-nanowire structure.

$$\rho_{NW} = R_{NW} \cdot \frac{A}{L}, \quad (2)$$

where R_{NW} is the resistance of an individual nanowire ($R_{NW} = R_T$ (total resistance) $- 2R_c$), and A is the nanowire cross-section area. Typical individual nanowire devices with an electrode distance of ~2 μm are shown in Fig. 3(a)–(f). The I–V characteristics of the various individual Au-peapodded silica nanowire devices exhibit typical Ohmic contact behavior [ESI, Fig. S1†].

We determined the resistivity of the nanowires according to the TML method as described in eqn (1) and (2). Fig. 3(g) shows the resistivity (ρ_{NW}) as a function of the number of Au-nanoparticles inside single silica nanowires of 1–3 μm in length at room temperature. It reveals that the dark conductivity can be controlled by tailoring the number of incorporated gold nanoparticles. The same Figure shows the inter-particle distance of the nanoparticles in the nanowire as a function of the number of gold nanoparticles. The majority of Au-nanoparticles have an inter-particle distance of about 200 nm, which can be attributed to the growth mode of the peapodded nanowire. The dark conductivity was found to increase with increasing numbers of embedded NPs in the silica nanowires. Since all of the single nanowire devices are fabricated by the same FIB process the dimension of the contacts are similar, as shown in Fig. 3(a)–(f). Therefore, the same contact resistance can be applied to derive R_{NW} in eqn (2), which results in the resistivity–particle number

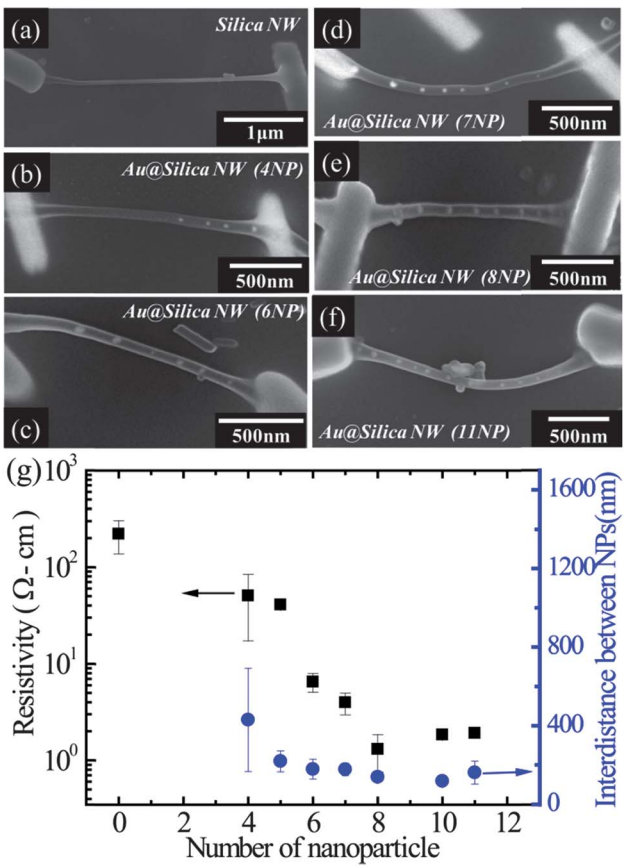

Fig. 3 (a–f) SEM images of the single silica nanowire devices with various numbers of embedded Au-NPs. (g) Resistivity and particle-to-particle distance of single silica nanowires measured as a function of the number of gold nanoparticles inside the silica nanowire.

relationship depicted in Fig. 3(g). In order to have better understanding of the phenomena, the transport behavior of dark conductivity in this hybrid 1D nanostructure was systemically investigated by temperature-dependent current–voltage measurements.

As the temperature decreases, the electrical carrier transport in disorder materials can be described by Mott's variable range hopping (VRH),[15] which is based on the hypothesis of an energy-independent density of state distributed near the Fermi level. For the Mott-VRH (3D) model, the resistivity can be expressed as

$$\sigma(T) = \sigma_o \exp\left[-\left(\frac{T_o}{T}\right)\right]^{1/4}, \quad (3)$$

where T_o is the characteristic Mott temperature and σ_o is the prefactor.

Recently Ke *et al.* have reported[16] the transport properties of silicon nanowires fabricated by FIB with Pt as the metal contact, which is similar to the nanowires presented here. They found that the changes in the contact resistivity were only several μΩ cm^2 in the temperature range from 100 K to 400 K. Thus, we can ignore the change in the contact resistance at different temperatures and derive the temperature-dependent conductivity using TLM to understand the transport mechanism in Au-peapodded nanowires.

Fig. 4(a) plots the logarithm of conductivity as a function of $T^{-1/4}$ for six specimens with different numbers of Au-nanoparticles in the nanowires. We determined $T_o^{1/4}$ and σ_o from the slope and intercept of the best-fit line in Fig. 4(a). It was concluded that the conductivity follows exponential temperature dependence according to Mott VRH model. However, the fitting parameters, such as the density of states at the Fermi level and hopping distance, (R_{Mott}), derived from Mott's hypothesis[17] exhibit nonphysical values, as shown in Table 1. Therefore, a revised Mott's model based on a localized density of state exponentially distributed above the Fermi level, and a band tail hopping model[18,19] was used to describe the system. The Motts' VRH model assumes that the density of state is constant at the Fermi level.[20] The band tail hopping presumes that hopping conduction between localized states is randomly distributed in space with an exponential density of state above the Fermi level, which can be described by

$$N(E) = N(E_F)e^{(E-E_F)/E_0}, \quad (4)$$

where $N(E_F)$ is the density of state and E_0 is the electronic disorder parameter.[20] For the band tail hopping model, the $T_o^{1/4}$ power law is similar to Mott's VRH (3D) model as described in eqn (3). The prefactor σ_o and $T_o^{1/4}$ can be obtained by the intercept and the slope, respectively, of the lines in Fig. 4(a).

The slope $T_o^{1/4}$ is related to the density of state at the Fermi level by the relationship

$$T_o = 310\left(\frac{\alpha^3}{k_B N(E_F)}\right), \quad (5)$$

where α^{-1} is the decay length of the electronic wave function about 11 Å[21] and k_B is the Boltzmann constant. The band tail hopping distance, R_{BT}, is approximated by[20]

$$N(E) \approx R_{BT}(E)^{-3}, \quad (6)$$

Fig. 4(b) shows the relationship between prefactor σ_o and $T_o^{1/4}$ deduced from eqn (3), wherein the red line corresponds to

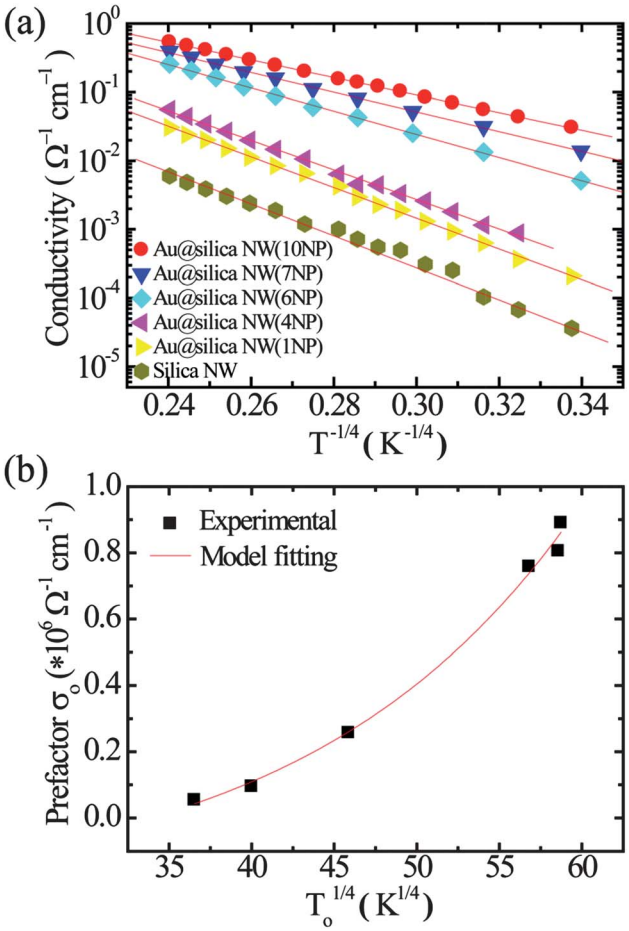

Fig. 4 (a) Variation of conductivity as a function of $T^{-1/4}$ for a single silica nanowire device with different numbers of gold nanoparticles inside the silica nanowire in the temperature range 77–300 K. (b) Prefactor σ_o as a function of $T_o^{1/4}$ for a variety of single gold peapodded silica nanowires. The red line indicates hopping modeled with an exponential tail state distribution.

modeling the typical band tail hopping within an exponential tail state distribution. This behavior contradicts the Mott-VRH model, which hypothesized an energy-independent $N(E_F)$ distribution.[18,22] In addition, the X-ray emission spectroscopy (XES) and X-ray absorption near-edge structure (XANES) spectra of the O 2p states of Au-NP embedded silica nanowires clearly show a band tail edge exponential distribution above the Fermi level.[23] Therefore, the mechanism of dark conductivity transport in the Au-peapodded silica nanowire is better described by the band tail hopping model.

Table 1 presents the calculated parameters based on the band tail hopping model described in eqn (3). The density of state and hopping distance, R_{BT}, are derived from eqn (5) and (6), respectively. The calculated results indicate that the conductivity increases with increasing density of state and decreasing hopping distance, R_{BT}.

The Au-NP embedded amorphous silica nanowires will create localized states such as defect states and interfacial sites to promote electron hopping conduction.[24] According to our earlier report,[11] the cathode luminescence (CL) spectra of the Au-peapodded silica nanowires had three defect peaks at 3.3, 3.0, 1.9 eV, which can be assigned to the luminescence of Si–O–C, ≡Si–O–Si≡, ≡Si–O,

Table 1 Parameters for single gold peapodded silica nanowires with different numbers of gold nanoparticles inside the silica nanowire. Prefactor σ_o and the slope T_o form the linear fit in Fig. 4(a). The density of states and hopping distance were estimated based on the Mott-VRH and band tail hopping model

Sample	Resistivity ρ (Ω cm) 300 K	T_o (K) (77–300 K)	Prefactor σ_o (Ω^{-1} cm^{-1})	Mott model		Band tail model	
				$N(E_F)$ (T = 300 K)	R_{Mott} (cm)	$N(E_F)$ (T = 300 K)	R_{BT} (cm)
NW (10 NPs)	1.87	1.78×10^6	5.41×10^4	2.21×10^{33}	1.24×10^{-11}	1.51×10^{21}	8.71×10^{-8}
NW (7 NPs)	2.55	2.56×10^6	9.57×10^4	1.46×10^{34}	6.40×10^{-12}	1.05×10^{21}	9.83×10^{-8}
NW (6 NPs)	4.72	4.42×10^6	2.57×10^5	3.76×10^{35}	2.07×10^{-12}	6.10×10^{20}	11.79×10^{-8}
NW (4 NPs)	17.23	1.04×10^7	7.59×10^5	1.47×10^{37}	5.69×10^{-13}	2.59×10^{20}	15.68×10^{-8}
NW (1 NP)	32.58	1.17×10^7	8.06×10^5	1.87×10^{37}	5.20×10^{-13}	2.29×10^{20}	16.34×10^{-8}
Silica NW	169.82	1.19×10^7	8.90×10^5	2.54×10^{37}	4.96×10^{-13}	2.26×10^{20}	16.41×10^{-8}

respectively. Possible interfacial states and defects states (Si–O–C, ≡Si–O–Si≡, ≡Si–O) were located at the interface between the gold nanoparticle and silica and in the amorphous silica nanowire. The electron hopping from occupied state to empty state can be enhanced by creating more density of states. On the other hand, according to the growth mechanism of Au-NP peapodded silica nanowires,[11] some gold atoms may diffuse into the silica wire during the peapod formation process. Therefore, the number of gold nanoparticles embedded increases as the amount of gold atoms in the wire increases. The Au-NPs may act as hopping sites and lead to enhanced conductivity.

This significantly enhanced conduction of silica nanowires can be used for sensing applications, because the charge transferred carriers during sensing can be easily conducted through the nanowire and finally collected by electrodes. As shown in Fig. 5, the oxygen sensing response with various pressures for single plain silica nanowires and single Au-peapodded silica nanowires was measured. The sensing response was defined by following equation:

$$\text{response} = \frac{I_{Vac} - I_{O_2}}{A_{NW}} \left(\text{A m}^{-2}\right), \quad (7)$$

where A_{NW} is the surface area of a single nanowire. The sensing response of Au-peapodded silica nanowires was about 20 times higher than the plain silica nanowires.

These results support our hypothesis, in which higher conductivity Au-embedded silica nanowires exhibit better gas sensing responsivity.

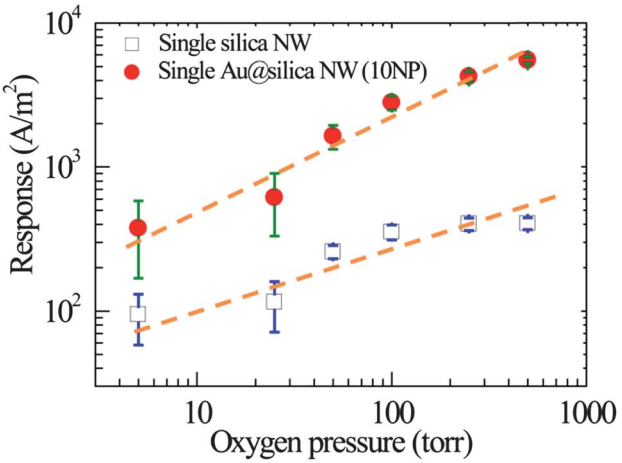

Fig. 5 Sensing response as a function of oxygen pressure for single silica nanowire and single Au@silica nanowires.

It has been reported that the conductance of nanowires will decrease in the presence of oxygen molecules according to the reaction: $O_2(g) + e^- \rightarrow O_2^-$ (ad),[25] which is the mechanism for its oxygen sensing. Higher conductivity means a higher carrier (e^-) concentration in Au-peapodded nanowires, which results in an enhanced response. An enhanced response is observed not only for the peapodded nanowire, but also a higher slope in Fig. 5, indicating higher sensitivity for Au-peapodded nanowires than regular ones for oxygen detection. It suggests that the metal nanoparticles embedded in amorphous nanowires provide a new approach to enhance not only the electron conduction, but also the chemical/bio-sensor response/sensitivity.

Conclusion

We have studied the temperature-dependent electrical transport properties of individual gold-peapodded amorphous silica nanowires synthesized by MWPECVD. It was found that the dark conductivity of the peapodded nanowires is strongly correlated with the number of particles incorporated and the electron transport in the nanowires is dominated by the band tail hopping process. The incorporated Au-NPs increases the number of hopping sites formed during nanowire growth and leads to enhanced conductivity. Consequently, the conductivity of the nanowires can be modulated by the number of incorporated NPs. The significant enhancement of the conductivity is also demonstrated to improve the chemical sensor performance of the nanowires. This result has provided a new approach for future applications in chemical/bio sensors, SPR sensors, optoelectronic devices and semiconductor devices.

Acknowledgements

This work was supported by the Ministry of Education, the National Science Council, National Cheng Kung University (NCKU), Taiwan and Academia Sinica, Taiwan. This work was also supported by the Center for Condensed Matter Sciences (CCMS), National Taiwan University. Technical support was provided by the Core Facilities for Nano Science and Technology, Academia Sinica and the National Taiwan University.

Notes and references

1 P. Mazzoldi, G. W. Arnold, G. Bertoncello, R. Bertoncello and F. Gonella, *Nucl. Instrum. Methods Phys. Res., Sect. B*, 1994, **91**, 478–492.
2 G. W. Arnold, G. D. Marchi, F. Gonella, P. Mazzoldi, A. Quaranta, G. Battaglin, M. Catalano, F. Garrido and R. F. Haglund, Jr, *Nucl. Instrum. Methods Phys. Res., Sect. B*, 1996, **116**, 507–510.

3 M. A. Noginov, G. Zhu, A. M. Belgrave, R. Bakker, V. M. Shalaev, E. E. Narimanov, S. Stout, E. Herz, T. Suteewong and U. Wiesner, *Nature*, 2009, **460**, 1110–1112.
4 K. Xu, L. Qin and J. R. Heath, *Nat. Nanotechnol.*, 2009, **4**, 368–372.
5 A. V. Moskalenko, S. N. Gordeev, O. F. Koentjoro, P. R. Raithby, R. W. French, F. Marken and S. E. Savel'ev, *Phys. Rev. B: Condens. Matter Mater. Phys.*, 2009, **79**, 241403.
6 P. Y. Lai and J. S. Chen, *Appl. Phys. Lett.*, 2008, **93**, 153305.
7 J. S. Lee, J. Cho, C. Lee, I. Kim, J. Park, Y. M. Kim, H. Shin, J. Lee and F. Caruso, *Nat. Nanotechnol.*, 2007, **2**, 790–795.
8 S. Link, M. B. Mohamed and M. A. El-Sayed, *J. Phys. Chem. B*, 1999, **103**, 3073–3077.
9 H. Han, N. D. Theodore and T. L. Alford, *J. Appl. Phys.*, 2008, **103**, 013708.
10 A. Devenyi, R. Manaila-Devenyi and R. M. Hill, *Phys. Rev. Lett.*, 1972, **29**, 1738–1741.
11 M. S. Hu, H. L. Chen, C. H. Shen, L. S. Hong, B. R. Huang, K. H. Chen and L. C. Chen, *Nat. Mater.*, 2006, **5**, 102–106.
12 C. H. Hsieh, L. J. Chou, G. R. Lin, Y. Bando and D. Golberg, *Nano Lett.*, 2008, **8**, 3081–3085.
13 P. H. Chen, C. H. Hsieh, S. Y. Chen, C. H. Wu, Y. J. Wu, L. J. Chou and L. J. Chen, *Nano Lett.*, 2010, **10**, 3267–3271.
14 J. S. Wu, S. Dhara, C. T. Wu, K. H. Chen, Y. F. Chen and L. C. Chen, *Adv. Mater.*, 2002, **14**, 1847–1850.
15 V. F. Gantmakher, *Electrons and Disorder in Solids*, Oxford University Press, Oxford, 2005.
16 J. J. Ke, K. T. Tsai, Y. A. Dai and J. H. He, *Appl. Phys. Lett.*, 2012, **100**, 053503.
17 D. K. Paul and S. S. Mitra, *Phys. Rev. Lett.*, 1973, **31**, 1000–1003.
18 C. Godet, *Philos. Mag. B*, 2001, **81**, 205–222.
19 P. Achatz, O. A. Williams, P. Bruno, D. M. Gruen, J. A. Garrido and M. Stutzmann, *Phys. Rev. B: Condens. Matter Mater. Phys.*, 2006, **74**, 155429.
20 C. Godet, *Phys. Status Solidi B*, 2002, **231**, 499–511.
21 S. J. Bending and M. R. Beasley, *Phys. Rev. Lett.*, 1985, **55**, 324–327.
22 C. Godet, *J. Non-Cryst. Solids*, 2002, **299–302**, 333.
23 C.-W. Pao, C.-T. Wu, H.-M. Tsai, Y.-S. Liu, C.-L. Chang, W. F. Pong, J.-W. Chiou, C.-W. Chen, M.-S. Hu, M.-W. Chu, L.-C. Chen, C.-H. Chen, K.-H. Chen, S.-B. Wang, S.-J. Chang, M.-H. Tsai, H.-J. Lin, J.-F. Lee and J.-H. Guo, *Phys. Rev. B: Condens. Matter Mater. Phys.*, 2011, **84**, 165412.
24 V. Ng, H. Ahmed and T. Shimada, *Appl. Phys. Lett.*, 1998, **73**, 972.
25 H. Kind, H. Q. Yan, B. Messer, M. Law and P. Yang, *Adv. Mater.*, 2002, **14**, 158–160.

